ABSTRACT

Chromosome segregation must occur with fidelity to maintain genome stability and prevent aneuploid disorders. During segregation, the kinetochore is assembled onto centromeric DNA and achieves the attachment of microtubule plus ends, which provide the force to physically segregate chromosomes to opposite poles of the cell. The kinetochore is a macromolecular protein/DNA machine composed of 8-9 biochemical complexes, the DNA-binding components of which define the inner kinetochore, and the microtubule-binding components of which define the outer kinetochore. The 3D protein architecture of the inner kinetochore in living cells remains poorly understood due to the resolution limits of live-cell imaging techniques. Here, we use pairwise, *in vivo* fluorescence microscopy to determine the position of kinetochore components relative to the centromere specific histone H3 variant, Cse4, with nanometer resolution. In addition, we complement kinetochore focus analysis with DNA dynamics simulations to propose a connection between chromatin dynamics and the observed anisotropy of the inner kinetochore proteins, Ame1 and Cse4, relative to the outer kinetochore proteins, Ndc80 and Nuf2.

INTRODUCTION

The centromere is the region of the chromosome responsible for the segregation of chromosomes to opposite poles during mitosis. In the budding yeast *saccharomyces cerevisiae,* the centromeric DNA spans a ~150 bp region that associates with the histone H3 variant Cse4, specifying kinetochore assembly (Biggins 2013). The kinetochore physically links chromosomes to spindle microtubule (MT) plus ends. It functions to hold sister chromatids together until proper chromosome biorientation has been achieved and couples the force of MT polymerization and

depolymerization to chromosome segregation (Pearson *et al*. 2001; Santaguida and Musacchio 2009; Joglekar *et al.* 2010).

These functions are related to the specific arrangement of individual protein components on the DNA surface. The small size of the kinetochore has made it difficult to accurately visualize these structures in living cells using microscopy. One kinetochore is roughly 68 nm in length and 35 nm in diameter (Joglekar *et al.* 2009). Furthermore, one spindle contains 16 kinetochores that cannot be distinguished from each other. Tagged kinetochores form a single focus until metaphase, when they separate into two foci (Goshima and Yanagida 2000; He *et al.* 2000; Pearson *et al.* 2001). While the kinetochore-MT interface has been well characterized, the nature of kinetochore attachment on chromatin remains poorly understood. Knowing the structure of the kinetochore at the centromere in living cells will be critical to understanding mechanisms responsible for kinetochore function.

Mammalian kinetochores attach to multiple microtubules (20-25); In contrast, budding yeast kinetochores assemble on "point centromeres," with each kinetochore attaching to a single spindle microtubule. The entire spindle contains 40 microtubules, including the 32 kinetochore microtubules and 8 interpolar microtubules (Santaguida and Musacchio 2009; Biggins 2013). The kinetochore is assembled from 8-9 distinct multicomponent complexes: CBF3, Ndc80, MIND, Spc105, Ctf19, DASH, Mif2 and COMA. Here, we define the inner kinetochore as the components that closely associate with centromeric DNA, and the outer kinetochore as those that associate with microtubules. The region spanning sister kinetochores is called the pericentromere. It is enriched in the SMC proteins cohesin and condensin, which organize DNA into compact loops (Yeh *et al.* 2008). While the kinetochores of yeast are simplified compared to

those found in other eukaryotes, most of the core components are conserved (Cheeseman and Desai 2008; Joglekar *et al.* 2008, 2009; Santaguida and Musacchio, 2009).

The stereotypic nature of the kinetochore makes statistical analyses of the mitotic spindle feasible. While individual subunits are below the diffraction limit of 25 nm, the use of Gaussian fitting to determine centroids of associated fluorophore distributions has enabled mapping of the position of kinetochore proteins along the spindle axis with nanometer accuracy (Joglekar *et al*. 2009). In this study, we use a pairwise, super-resolution fluorescence microscopy method and chromatin dynamics simulations paired with a microscope simulator to gain new insights into the structure of the budding yeast inner kinetochore.

Electron micrographs of kinetochores show a structure that narrows to a dense cluster surrounding Cse4 (Gonen *et al.* 2012, Dimitrova *et al*. 2016). *In vivo*, the inner kinetochore complex COMA (Ame1) and Cse4 produce a focus that is more extended perpendicular to the spindle axis (anisotropic) than those produced by the outer kinetochore components Ndc80 and Nuf2 (Hasse *et al.* 2012). In the case of Cse4, this anisotropy is dependent on Pat1 and Xrn1 and therefore represents the presence of additional molecules around the centromere (Lawrimore *et al.* 2010; Hasse *et al.* 2013). Because the anisotropic focus produced by Ame1 is unaffected by Pat1 or Xrn1 deletions, it must be accounted for by another mechanism (Hasse *et al.* 2013).

Experimental evidence and computer modeling support the idea that tension produced when sister kinetochores achieve biorientation is important for maintaining kinetochore-MT attachments (Gardner *et al.* 2005, Franck *et al*. 2007; Akiyoshi *et al*. 2010). The cell monitors this tension to identify and correct errors arising during the formation of attachments (Nicklas

and Koch 1969; Nicklas 1997). Previously, a physically accurate chromatin simulator has been used to show that the formation of DNA loops by condensin and cohesin creates tension along the pericentromere (Lawrimore *et al.* 2015). In addition, a deletion in either Bub1, a component of the spindle assembly checkpoint (SAC), or Sgo1, a protector of cohesion, is coincident with a loss of anisotropy at the inner kinetochore (Hasse *et al.* 2012). Taken together, these two findings suggest that changes in tension at the pericentromere may be associated with structural changes in the kinetochore.

Here, we demonstrate that experimentally determined kinetochore position and focus dimensions can be recapitulated using a chromatin dynamics simulator run through a microscope simulator. This finding provides a feasible method for testing whether different chromatin configurations and conditions are consistent with kinetochore structural features observed using live-cell light microscopy.

EXPERIMENTAL METHODS

Strains and Growing Conditions

Strains (Table 1) were grown in complete medium with a glucose carbon source at 32 °C. Homologous recombination was used to tag kinetochore proteins with GFP or RFP. With the exception of Cse4 and Ndc80, all kinetochore proteins were tagged at the C-terminus. Cells were grown to mid-log phase and re-suspended in synthetic media + 2% glucose immediately prior to imaging.

Table 1. List of strains and plasmids used in study

Strain	Genotype	Source
YEF473A	trp1Δ 63 leu2Δ ura3-52 his3Δ 200 lys2-8 Δ 1	K.Bloom
PH499A	ura3-52, lys2-801, ade2-101, his3Δ200, leu2Δ1, trp1Δ63	Phil Hieter
YBM536	PH499 + ndc10 K556R, K651R, K652R, K7799R-GFP::HIS	Phil Hieter
YPH1820	YBM1820 Cep3-GFP:HIS3	Phil Hieter
pRB920 cut	2xGFP-Cse4:TRP1	R. Baker
pKS390	pFA6a-mCherry:kanMX6	K. Bloom
pKS391	pFA6a-mCherry:natMX6	K. Bloom
DCY1100	YEF473A + 2xGFP-Cse4:TRP1	K. Bloom
DCY1101	DCY1100 + Ame1-mCherry:KAN^r	K. Bloom
DCY1102	DCY1100 + Mtw1-mCherry:KAN^r	K. Bloom
DCY1038	KBY7999 + 2xGFP-Cse4:TRP1	K. Bloom
DCY1045	DCY1038 + Dsn1-cerulean:NAT^r	K. Bloom
DCY1110	YBM536 + Ame1-mCherry:NAT^r	K. Bloom
DCY1111	YPH1820 + Ame1-mCherry:NAT^r	K. Bloom
DCY1115	(cen3(3.8)) + Ame1-mCherry:NAT^r	K. Bloom
DCY1116	(cen15(1.8)) + Ame1-mCherry:NAT^r	K. Bloom
DCY1118	DCY1100 + Nnf1-mCherry:NAT^r	K. Bloom
DCY1136	DCY1100 + Ctf19-mCherry:KAN^r	K. Bloom
DCY1141	DCY1100 + Chl4-mCherry:KAN^r	K. Bloom
KBY6326	DCY1100 + Slk19-mCherry:NAT^r	K. Bloom
KBY7040	YEF473A + Ndc80-tdTomato:NAT^r	K. Bloom
KBY7042	KBY9345.1 + Cyc1-GFP-Ndc80:NAT^r	K. Bloom
KBY7043	KBY7042 + Spc24-tdTomato:KAN^r	K. Bloom
KBY7999	YEF473A + Spc29-RFP:Hb	K. Bloom
KBY8745	KBY7999 + Ame1-GFP: KAN^r	K. Bloom
KBY9345	YEF473A + Cyc1-GFP-Ndc80:NAT^r	K. Bloom
KBY9453	KBY7999 + Ndc80-tdTomato:NAT^r	K. Bloom
KBY9496	KBY7999 + Cse4-2xGFP:TRP1	K. Bloom

KBY8116	KBY7999 + Ndc80-GFP:KAN^r	K. Bloom
KBY9075	KBY7999 + Nuf2-GFP:URA3	K. Bloom

Imaging

To determine kinetochore protein axial positions, population images of strains containing Cse4 (GFP) and kinetochore components (RFP) were imaged at room temperature (25°C) using an Eclipse E600FN microscope (Nikon) with a 100× Plan Apo TIRF 1.45 NA objective (Nikon) and ImagEM EM-CCD digital camera (Hamamatsu) with a custom Lumencor LED illumination system (Lumencor Inc.) using MetaMorph 7.7 imaging software (Molecular Devices). To characterize kinetochore component focus shape, strains containing spindle pole body proteins (Spc29-RFP) and kinetochore components (GFP) were imaged at room temperature (25°C) on a Nikon TE2000, widefield, 100X 1.4 NA Orca II with MetaMorph software. Each acquisition was a 7-step Z-stack with a 300-nm step size in the GFP, RFP, and Trans channels.

Image Analysis

Custom software written with MatLAB R2017 was used to extract the location of kinetochore foci from microscope images. Brightest regions for GFP and RFP spots were manually selected, and a 7x7 pixel region was automatically applied to the surrounding area. Centroids of kinetochore foci were mathematically determined using “brightest pixel” and Gaussian fitting methods.

To map kinetochore protein position along the spindle (x-axis), we use the centromere specific nucleosome variant Cse4 as a fiducial. The x-axis is defined by rotating the GFP channel until

the brightest pixel for one Cse4 focus is horizontal to the brightest pixel for the opposite Cse4 focus. The RFP channel representing the tagged kinetochore proteins is then rotated by the same degree. Cse4 is set at 0, and measurements are made relative to this position. Pixel measurements are converted to distance based on pixel size (64.8 nm). To account for spindle tilt, cells with kinetochores at opposite poles differing by more than 600 nm in Z were excluded. Position analysis was limited to metaphase cells by imposing limits of 200-1200 nm for RFP-RFP and GFP-GFP focus distances. Methods for x-position analysis are further outlined in Figure 1.

To determine the extension of the foci produced by kinetochore proteins perpendicular to the spindle (y-axis), spindle pole bodies are used as a fiducial. The RFP channel is rotated until the brightest pixel for one spindle pole body) is horizontal to the brightest pixel for the opposite Cse4 focus. Once the spindle is aligned, the spindle poles are set at 0,0, and the GFP channel representing the kinetochore proteins is rotated by the same degree. The full width at half maximum (FWHM) of the one-dimensional Gaussian distribution fitted to each GFP focus is determined to measure extension in y. Methods for FWHM determination are outlined in Figure 2.

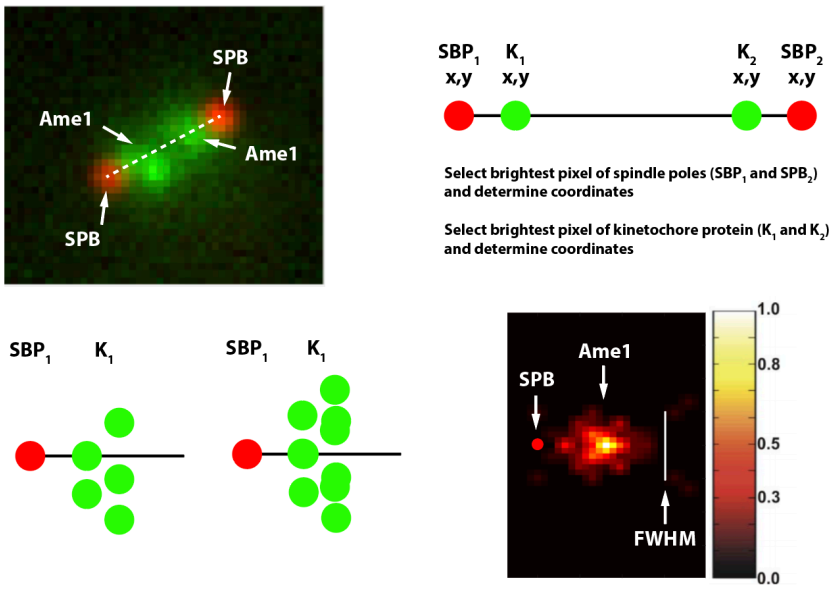

Figure 1. Outline of methods used to determine x-position of kinetochore proteins along the spindle axis.

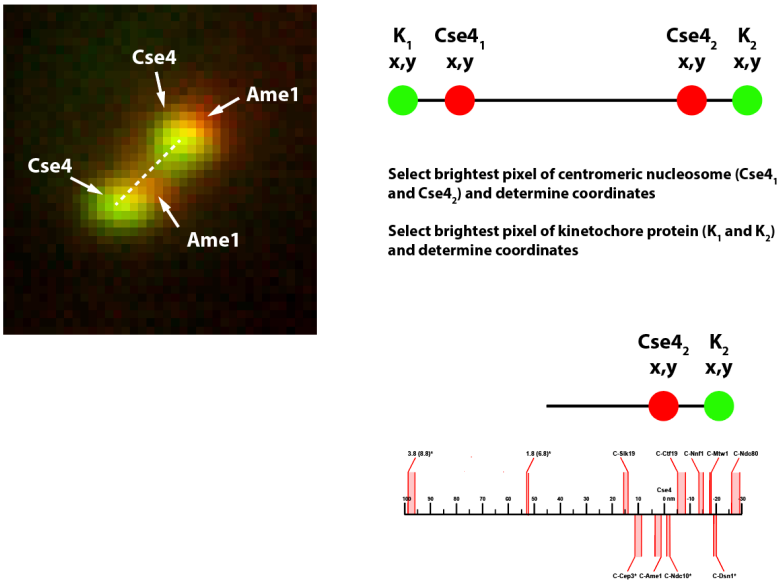

Figure 2. Outline of methods used to determine FWHM of kinetochore proteins perpendicular to the spindle axis.

RESULTS

Nanometer localization of kinetochore components

During metaphase, kinetochores from sister chromatids are bioriented and appear as two separate foci along the mitotic spindle axis. Each spot represents a cluster of 16 kinetochore copies, with one kinetochore per spindle microtubule. Two-color, pairwise imaging was performed on populations of metaphase cells to determine the spatial organization of individual kinetochore proteins. We compared different kinetochore components labeled with RFP to Cse4 labeled with two molecules of GFP. This Cse4-GFP double fusion fully complements a Cse4 null mutation (Baker *et al.* 2013, Lawrimore *et al.* 2011, Wisneiski *et al.* 2015). Custom software was used to manually select centroids of spots and extract positional information from the image. Measurements were determined along the axis extending between Cse4 spots at opposite poles, which roughly approximates the orientation of the spindle axis. For some kinetochore proteins, position was determined relative to Ame1 (RFP), which is within 2-4 nm of Cse4 (Figure 1). In this case, the kinetochore protein in question was labeled with GFP.

Two methods of centroid localization were employed in this study: “brightest pixel” picking and Gaussian fitting. Statistically, the brightest pixel is most likely to occur at the center of a Gaussian distribution. Therefore, it can be used to approximate the average location of the labeled kinetochore components. Because this method is less stringent than Gaussian fitting, we can acquire a larger sample size. We confirmed the accuracy of the brightest-pixel method by comparing the axial distance of Ndc80, a rod-like outer kinetochore protein, relative to Cse4 and the outer kinetochore protein Spc24 to it’s known length of 57 nm. Our results for the two methods differ by less than 3 nm from one another in all cases except for N-Ndc80 (RFP) and C-

Spc24 (GFP). Our protein-protein distances confirm previously reported measurements, giving further support for our method (Joglekar *et al*. 2009; Hasse *et al.* 2013). The consistency between the two methods in this study and our ability to reproduce results from prior studies indicate that "brightest pixel" selection of centroids is accurate compared to Gaussian fitting.

On average, the outer kinetochore protein Ndc80 (C-terminally labeled) is 26-29 nm from Cse4 (toward the microtubule). The middle kinetochore MIND complex (Mtw1, Nnf1, Dsn1) is ~13-20 nm from the Cse4 nucleosome (toward the microtubule). The inner kinetochore complex CBF3 (Cep3, Ndc10) is ~1-10 nm from Cse4. The inner kinetochore complex COMA (Ame1) is within 1-4 nm of Cse4 (toward the pericentromere). The inner centromere protein, Slk19 is 14-17 nm from Cse4 (toward the pericentromere.) DNA in the pericentromere, represented by 8.8 and 6.8-kb LacO/LacI-GFP arrays, is 99 and 53 nm away from Cse4, respectively (Figure 31, Table 2).

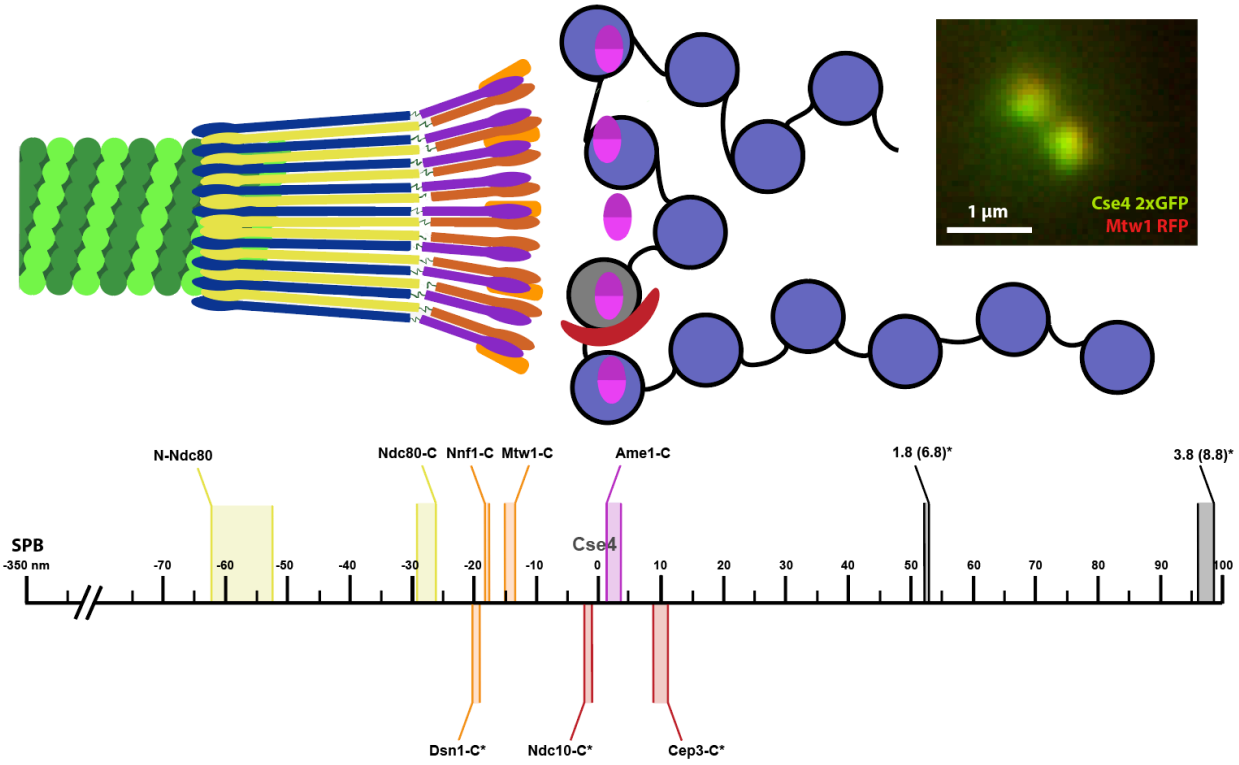

Figure 3. Average metaphase locations of DNA (8.8, 6.8-kb LacO/LacI-GFP array) and kinetochore proteins (Slk19, Cep3, Ame1, Ndc10, Nnf1, Dsn1, Mtw1, Ndc80) along the Cse4-Cse4 axis (n= 78 for Ndc80, n=~200 for others). DNA/proteins whose position was determined relative to Ame1 (RFP) are denoted with an asterisk. Each red box represents the difference between the average distances measured using brightest-pixel and Gaussian fitting methods. Protein names are labeled at the line corresponding to the distance acquired using Gaussian fitting. (Cooke and Drysdale, unpublished.)

Table 2. Raw position data for kinetochore proteins along the inner kinetochore axis (Cse4-Cse4 or Ame1-Ame1, x-axis) and mean distance between Cse4 (GFP) and kinetochore protein (RFP) foci determined using brightest pixel (BP) and Gaussian fitting centroid determination methods. Cells fit with a Gaussian for centroid determination represent a subset of those for which BP method was used. Negative values indicate positions on the MT side of Cse4 or Ame1. RFP-GFP distances are determined by taking the absolute values of position measurements. Numbers of cells used for BP method are between 100-300, with the exception of the strain containing N-Ndc80 and C-Spc24.

RFP	GFP	Method	n	Mean x-position (nm)	STD (nm)	Mean RFP-GFP distance (nm)	STD (nm)
Ame1	Cen3 (3.8)	BP	212	96.7770	96.2706	109.6746	81.1952
		Gaussian	57	99.2945	92.0368	108.7433	80.4361
Ame1	Cen15 (1.8)	BP	179	53.6141	92.8861	86.1189	63.7206
		Gaussian	111	53.7198	89.7948	82.4906	64.0984
Ame1	Ndc10	BP	200	-1.8548	70.9117	54.5949	45.1258
		Gaussian	39	-2.4465	47.0174	31.7369	34.3954
Ame1	Cep3	BP	181	9.3010	77.9731	60.9371	49.3237
		Gaussian	18	11.7759	38.0423	27.4896	28.1765
Dsn1	Cse4	BP	224	-19.6763	62.5296	48.4556	44.0496
		Gaussian	122	-20.3900	43.2502	36.6611	30.5716
Ame1	Cse4	BP	172	4.4423	62.3717	47.2885	40.7529
		Gaussian	80	1.2095	39.1846	28.7643	26.4397
Mtw1	Cse4	BP	133	-15.0765	54.1906	41.6191	37.6878
		Gaussian	120	-18.5278	36.8174	31.4320	26.5597
C-Nnf1	Cse4	BP	110	-17.3079	76.3839	61.8698	47.6847
		Gaussian	26	-13.1923	43.5081	33.2730	30.3739
C-Slk19	Cse4	BP	290	16.5674	75.4072	60.4478	47.9073
		Gaussian	162	14.2663	61.5573	45.8023	43.3960
C-Spc24	N-Ndc80	BP	78	47.2387	57.6011	60.7298	42.9228
		Gaussian	64	57.0025	34.3290	58.8171	31.0641
C-Ndc80	Cse4	BP	124	-29.2838	59.7482	50.6987	42.9313
		Gaussian	101	-26.4643	40.3034	40.7146	25.6412

Characterization of inner kinetochore focus shape shows anisotropy of Ame1 and Cse4

We imaged strains labeled with kinetochore proteins in GFP and spindle pole bodies (Spc29) in RFP for kinetochore focus size measurements. FWHM Measurements were made perpendicular to the axis defined by the spindle pole bodies (y-axis). The foci produced by Ndc80 and Nuf2 have a FWHM of ~375 nm in y. Ame1, a subunit of the inner kinetochore complex COMA, has a FWHM of 405 nm in y, and the centromere specific nucleosome Cse4 has a FWHM of 417 nm in y. The inner kinetochore components Ame1 and Cse4 show a more extended focus in y than the microtubule-bound, outer kinetochore components Ndc80 and Nuf2. The common fiducial used for this analysis, the spindle pole body component Spc29, has a consistent spot distribution in y across different strains, giving confidence to our method (Table 3). These FWHM values are mapped on top of probability density distribution maps that show the location of the brightest pixel measurements relative to the spindle pole body. Visually, the maps recapitulate our measurements, becoming physically more spread out moving away from the microtubule (Figure 4).

GFP	RFP	GFP Mean FWHM (nm)	RFP Mean FWHM (nm)	n
N-Ndc80	Spc29	375.34752	308.6424	126
C-Ndc80	Spc29	378.89208	309.62736	130
N-Nuf2	Spc29	374.9652	293.1228	198
C-Ame1	Spc29	404.40384	295.04736	60
C-Cse4	Spc29 (CFP)	417.96648	256.40712	84

Table 3. Full width half max (FWHM) in y of Gaussian distribution applied to brightest pixel of foci corresponding to kinetochore components. The foci produced by Spc29 have a consistent size across different strains, with the exception of the strain containing Cse4, which has Spc29 labeled with CFP. Perpendicular to the spindle axis, the foci produced by Ame1 are extended on average ~30 nm more than the foci produced by the outer kinetochore components Ndc80 and Nuf2. Cse4 is extended more than ~45 nm than the outer kinetochore components. Totals represent number of individual foci examined, or 2 foci per cell (Hasse and Drysdale, unpublished).

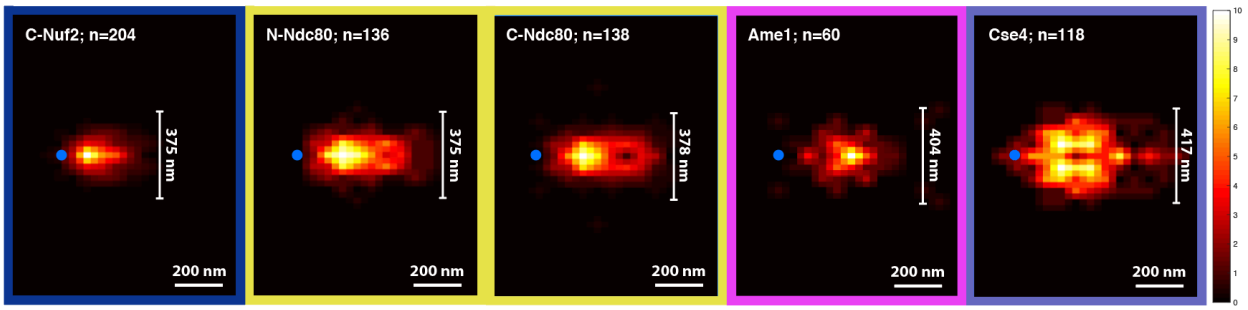

Figure 4. Probability density maps and FWHM values of outer kinetochore proteins Nuf2 and Ndc80 and inner kinetochore components Ame1 and Cse4 relative to the spindle pole body. The location of the spindle pole bodies is indicated by the blue dots.

Polymer models of the pericentromere simulate inner kinetochore spatial and dynamic features

The nature of the chromatin substrate must be incorporated into our understanding of inner kinetochore structure and function. We assume that the innermost complex of the kinetochore, COMA, is directly bound to DNA. Therefore, chromatin dynamics should have a direct impact on the distribution of COMA *in vivo*. We model the motion of the pericentromere using ChromoShake, a polymer dynamics simulator. The program subjects a string of beads linked by springs and hinges to Brownian motion in order to explore possible thermodynamic states (Lawrimore et al., 2016). Each bead is 10 nm in diameter and corresponds to roughly 30 bp of B-form DNA. The model accurately represents centromere dynamics in budding yeast mitosis (Lawrimore et al., 2016).

In our simulation, chromatin at the centromere is represented as rings of varying radii. The simulation is run through a microscope simulator to produce images that can be compared to experimentally obtained images. The foci produced using the microscope simulator are measured using the same image analysis method as the experimental images to allow us to directly match simulated and experimental FWHM data (Figure 5). We find that circles with radii of 127 and 130 nm recapitulate the experimental FWHM measurements for N-Ndc80 and C-Ndc80,

respectively. A radius of 127 nm corresponds to Nuf2. A radius of 142 nm corresponds to Ame1, and a radius of 147 nm corresponds to Cse4 (Table 4). These measurements are consistent with the radius of a microtubule, which is known to be 125 nm. Ndc8 and Nuf2 are tightly bound to the microtubule, and correspond to nearly the same radius.

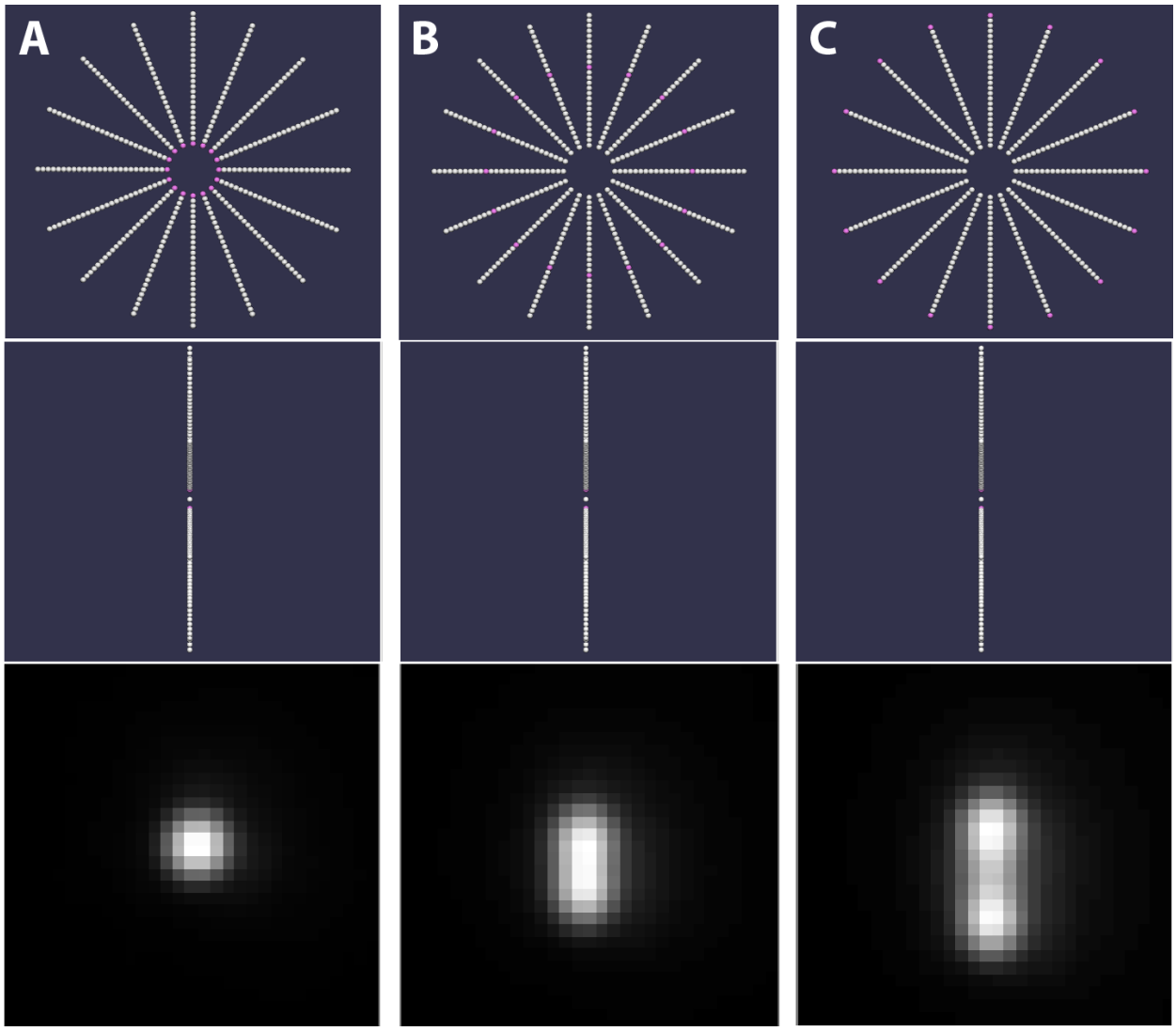

Figure 5. Chromatin dynamics simulator and corresponding microscope simulator image with rings of 16 DNA beads arranged in rings corresponding to 50 nm (A), 150 nm (B), and 300 nm (C) radii All images represent one half of a symmetric spindle. Chromatin dynamics simulator images represent starting arrangements before being subjected to Brownian motion. Beads labeled with magenta appear fluorescent in the microscope images. Top panel represents spindle end-on view, middle panel represents side on view, and lower panel is microscope simulation produced by fluorescently labeled beads. Microscope simulator images represent one time-step.

Circle Radius (nm)	Mean FWHM (nm)	n
50	292.7312288	493
60	306.2807663	493
70	314.8392064	490
80	328.2387803	497
90	337.5674121	494
100	352.7609542	497
110	366.958018	499
120	382.681577	499
130	402.9605773	500
140	417.4179623	499
150	439.5611626	500
160	460.1219686	500
170	474.7997901	500
180	499.6775509	500
190	515.7482014	500
200	539.6529136	500
210	561.1080588	500
220	582.5750472	500
230	602.875172	500
240	627.4962933	500
250	648.8479345	500
260	672.0738617	500
270	705.0916174	500
280	728.2658448	500
290	750.5365376	500
300	776.5703655	500

Table 4. Average FWHM in Y of Gaussian distribution applied to brightest pixel of foci produced by DNA loops of varying radii in microscope simulator images. Each simulation was performed ~500 times (Brandon Friedman, unpublished).

DISCUSSION

The kinetochore couples the force of dynamic microtubules to DNA, ensuring the proper segregation of chromosomes during cellular division. Kinetochore protein structure and architecture has been closely examined at the kinetochore-MT attachment site, but the arrangement of individual kinetochore proteins at the DNA surface remains poorly understood (Cheeseman and Desai 2008; Joglekar *et al*. 2009, 2010; DeLuca 2011). Super-resolution microscopy has been used to accurately describe the 3D location of fluorescently tagged kinetochore proteins in dividing cells (Joglekar *et al*. 2009; Hasse *et al*. 2013.)

This study contributes to our understanding of kinetochore architecture in budding yeast by mapping the location of the Ndc80 (Ndc80), MIND (Dsn1, Nnf1, Mtw1), COMA (Ame1), and CBF3 (Cep3, Ndc10) complexes, the inner centromere protein Slk-19, and pericentric DNA (8.8, 6.8-kb LacO/LacI-GFP arrays) along the Cse4-Cse4 axis. The signal-to-noise ratio of the image limits the accuracy of centroid localization that can be obtained using this method. Based on similar studies, we can expect a precision of ~10 nm for the lowest signal-to-noise ratio conditions. Our axial measurements agree with those obtained in prior studies using a different fiducial, giving confidence to our findings (Joglekar *et al*. 2009).

Two alternative arrangements have been proposed to describe the shape of the inner kinetochore. One follows a "vertical" plan of assembly, in which the kinetochore is built from the inner kinetochore to the outer kinetochore, beginning at Cse4 and extending to the microtubule (Joglekar *et al*. 2009) (Figure 6A/B). If the kinetochore followed such a plan, with the inner kinetochore attaching directly to Cse4, the displacement of single kinetochore perpendicular to the microtubule would not exceed ~125 nm, the diameter of a spindle microtubule. By extension, the displacement of the entire 16 kinetochore cluster would not exceed that of the microtubule-

bound outer kinetochore components. A second plan proposes that the kinetochore components associate with H3 nucleosomes surrounding the central Cse4 nucleosome (Figure 6D). In this arrangement, the force from microtubules would be distributed across multiple contact points on the chromatin, whereas in the former arrangement the entire force transmitted by the kinetochore would converge on a single Cse4 nucleosome (Santaguida and Musacchio 2009).

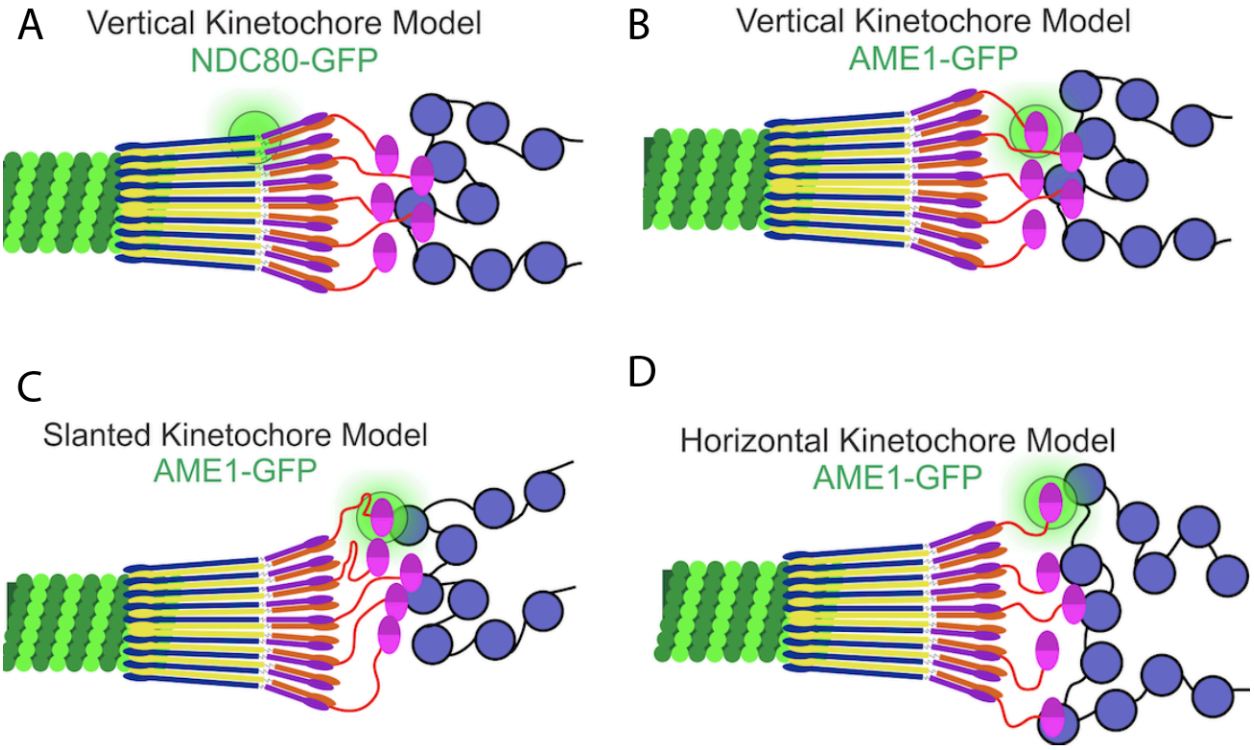

Figure 6. A.) Vertical kinetochore model with outer kinetochore protein showing Ndc80 labeled with GFP and B.) Vertical kinetochore model with inner kinetochore protein Ame1 labeled with GFP. C.) Slanted kinetochore model with centromeric DNA biasing inner kinetochore proteins away from the spindle axis. D.) Horizontal kinetochore model with inner kinetochore proteins uniformly splayed out on the face of the chromatin. Only the most radially displaced protein is labeled in all of these scenarios because only this protein would need to be skewed in such a way as to reproduce our FWHM results.

We attempt to distinguish between these two arrangements by extending our analysis in the direction perpendicular to the spindle axis. By comparing the FWHM in y of foci produced by

outer and inner kinetochore components, we find that the inner kinetochore is more extended perpendicular to the spindle axis than the outer kinetochore, recapitulating earlier findings (Hasse *et al.* 2013). This result is consistent with the second plan, in which the kinetochore flares out on the surface of the DNA and forms multiple attachments around Cse4. We complement our experimental microscopy findings with measurements from a simulator that explores different conformations of pericentric DNA. This simulation allows us to test how different inner kinetochore organizations combine with chromatin dynamics to produce images in a light microscope. We find that a series of rings with radii increasing by ~20 nm from the microtubule to the inner kinetochore recapitulate our experimental kinetochore foci when the simulation is fed through a microscope simulator.

Because we examine clusters of 16 kinetochores, we can only make conclusions about the structural qualities of individual kinetochores that would be reflected in the shape of the entire cluster. Another conformation that would explain our anisotropy and position findings would have all 16 kinetochores pointing at an angle away from the spindle axis (Figure 6C). Increased protein copy number at the centromere could also explain the extended foci, though it would have to be accounted by an alternative mechanism than the deletions that disrupt the observed anisotropy of Cse4 (Hasse *et al.* 2013). Using a chromatin simulation that equilibrates to the favored entropic state, we can test these conformations against what we observe in the microscope. This allows us to build intuition around how the thermodynamics and organization of chromatin combine with inner kinetochore architecture.

We plan to further test our hypothesis that the inner kinetochore flares out on the surface of the chromatin by examining how simulations of different possible inner kinetochore arrangements,

as well as increased protein copy number, combine with experimental position and FWHM information. In addition, this model provides a way for us to link large-scale changes in chromatin dynamics to small-scale changes in kinetochore architecture at the centromere. The same polymer dynamics simulator has been used previously to demonstrate that radial loops of chromatin generated by cohesion and condensin along the spindle axis generate tension in the pericentromere (Lawrimore *et al.* 2015). Other work has shown that Sgo1 and Bub1 are necessary to maintain the anisotropy observed in Ame1 and Cse4 (Hasse *et al.* 2012). Deletions in either of these proteins reduce tension in the pericentromere, indicating a possible connection between tension and kinetochore architecture. Such a tension-dependent structural change would also provide a mechanism by which the cell could possibly "sense" whether proper DNA attachment had been achieved and thus help regulate the spindle checkpoint.

CONCLUSIONS

We provide a map of kinetochore proteins relative to the Cse4 nucleosome along the spindle axis. In addition, we demonstrate that experimental kinetochore protein position and focus distribution can be recapitulated by simulated microscope images from a chromatin dynamics simulator. This finding provides a method for testing different chromatin configurations and conditions *in silico* against protein-protein distances and focus distributions observed *in vivo*. By allowing us to estimate where COMA interacts with DNA surrounding the Cse4 nucleosome, we hope to use this approach to explain the observed anisotropy of the inner kinetochore proteins, Ame1 and Cse4, relative to the outer kinetochore proteins, Ndc80 and Nuf2.

ACKNOWLEDGEMENTS

I would like to thank the members of the Bloom Lab, especially Kerry Bloom, Elaine Yeh, Josh Lawrimore, Diana Cooke, and Brandon Friedman and prior member of the Bloom lab Julian Hasse (NIH-NCI) for providing the image set used to determine kinetochore spot analysis. This work was supported by the NIH grant R3 GM32238 to K.B.

REFERENCES

Akiyoshi, Bungo, Krishna K. Sarangapani, Andrew F. Powers, Christian R. Nelson, Steve L. Reichow, Hugo Arellano-Santoyo, Tamir Gonen, Jeffrey A. Ranish, Charles L. Asbury, and Sue Biggins. "Tension Directly Stabilizes Reconstituted Kinetochore-Microtubule Attachments." *Nature* 468, no. 7323 (November 25, 2010): 576–79. https://doi.org/10.1038/nature09594.

Biggins, Sue. "The Composition, Functions, and Regulation of the Budding Yeast Kinetochore." *Genetics* 194, no. 4 (August 2013): 817–46. https://doi.org/10.1534/genetics.112.145276.

Boeckmann, L., Y. Takahashi, W.-C. Au, P. K. Mishra, J. S. Choy, A. R. Dawson, M. Y. Szeto, et al. "Phosphorylation of Centromeric Histone H3 Variant Regulates Chromosome Segregation in Saccharomyces Cerevisiae." *Molecular Biology of the Cell* 24, no. 12 (June 15, 2013): 2034–44. https://doi.org/10.1091/mbc.E12-12-0893.

Cheeseman, Iain M., and Arshad Desai. "Molecular Architecture of the Kinetochore–microtubule Interface." *Nature Reviews Molecular Cell Biology* 9, no. 1 (January 2008): 33–46. https://doi.org/10.1038/nrm2310.

DeLuca, K. F., S. M. A. Lens, and J. G. DeLuca. "Temporal Changes in Hec1 Phosphorylation Control Kinetochore-Microtubule Attachment Stability during Mitosis." *Journal of Cell Science* 124, no. 4 (February 15, 2011): 622–34. https://doi.org/10.1242/jcs.072629.

Dimitrova, Yoana N., Simon Jenni, Roberto Valverde, Yadana Khin, and Stephen C. Harrison. "Structure of the MIND Complex Defines a Regulatory Focus for Yeast Kinetochore Assembly." *Cell* 167, no. 4 (November 2016): 1014–1027.e12. doi:10.1016/j.cell.2016.10.011.

Franck, Andrew D., Andrew F. Powers, Daniel R. Gestaut, Tamir Gonen, Trisha N. Davis, and Charles L. Asbury. "Tension Applied through the Dam1 Complex Promotes Microtubule Elongation Providing a Direct Mechanism for Length Control in Mitosis." *Nature Cell Biology* 9, no. 7 (July 2007): 832–37. https://doi.org/10.1038/ncb1609.

Gardner, M. K. "Tension-Dependent Regulation of Microtubule Dynamics at Kinetochores Can Explain Metaphase Congression in Yeast." *Molecular Biology of the Cell* 16, no. 8 (May 18, 2005): 3764–75. https://doi.org/10.1091/mbc.E05-04-0275.

Goshima, Gohta, and Mitsuhiro Yanagida. "Establishing Biorientation Occurs with Precocious Separation of the Sister Kinetochores, but Not the Arms, in the Early Spindle of Budding Yeast." *Cell* 100, no. 6 (March 2000): 619–33. https://doi.org/10.1016/S0092-8674(00)80699-6.

Haase, Julian, Prashant K. Mishra, Andrew Stephens, Rachel Haggerty, Cory Quammen, Russell M. Taylor, Elaine Yeh, Munira A. Basrai, and Kerry Bloom. "A 3D Map of the Yeast Kinetochore Reveals the Presence of Core and Accessory Centromere-Specific Histone." *Current Biology* 23, no. 19 (October 2013): 1939–44. https://doi.org/10.1016/j.cub.2013.07.083.

Haase, Julian, Andrew Stephens, Jolien Verdaasdonk, Elaine Yeh, and Kerry Bloom. “Bub1 Kinase and Sgo1 Modulate Pericentric Chromatin in Response to Altered Microtubule Dynamics.” *Current Biology* 22, no. 6 (March 2012): 471–81. https://doi.org/10.1016/j.cub.2012.02.006.

He, X., S. Asthana, and P. K. Sorger. “Transient Sister Chromatid Separation and Elastic Deformation of Chromosomes during Mitosis in Budding Yeast.” *Cell* 101, no. 7 (June 23, 2000): 763–75.

Joglekar, Ajit P., Kerry Bloom, and E.D. Salmon. “In Vivo Protein Architecture of the Eukaryotic Kinetochore with Nanometer Scale Accuracy.” *Current Biology* 19, no. 8 (April 2009): 694–99. https://doi.org/10.1016/j.cub.2009.02.056.

Joglekar, Ajit P, Kerry S Bloom, and Ed Salmon. “Mechanisms of Force Generation by End-on Kinetochore-Microtubule Attachments.” *Current Opinion in Cell Biology* 22, no. 1 (February 2010): 57–67. https://doi.org/10.1016/j.ceb.2009.12.010.

Joglekar, Ajit P., David C. Bouck, Jeffrey N. Molk, Kerry S. Bloom, and Edward D. Salmon. “Molecular Architecture of a Kinetochore-Microtubule Attachment Site.” *Nature Cell Biology* 8, no. 6 (June 2006): 581–85. https://doi.org/10.1038/ncb1414.

Joglekar, Ajit P., David Bouck, Ken Finley, Xingkun Liu, Yakun Wan, Judith Berman, Xiangwei He, E.D. Salmon, and Kerry S. Bloom. “Molecular Architecture of the Kinetochore-Microtubule Attachment Site Is Conserved between Point and Regional Centromeres.” *The Journal of Cell Biology* 181, no. 4 (May 19, 2008): 587–94. https://doi.org/10.1083/jcb.200803027.

Lawrimore, Josh, Kerry S. Bloom, and E.D. Salmon. “Point Centromeres Contain More than a Single Centromere-Specific Cse4 (CENP-A) Nucleosome.” *The Journal of Cell Biology* 195, no. 4 (November 14, 2011): 573–82. https://doi.org/10.1083/jcb.201106036.

Lawrimore, J., J. K. Aicher, P. Hahn, A. Fulp, B. Kompa, L. Vicci, M. Falvo, R. M. Taylor, and K. Bloom. “ChromoShake: A Chromosome Dynamics Simulator Reveals That Chromatin Loops Stiffen Centromeric Chromatin.” *Molecular Biology of the Cell* 27, no. 1 (January 1, 2016): 153–66. doi:10.1091/mbc.E15-08-0575.

Nicklas, R. B. “How Cells Get the Right Chromosomes.” *Science (New York, N.Y.)* 275, no. 5300 (January 31, 1997): 632–37.

Nicklas, R. B., and C. A. Koch. “Chromosome Micromanipulation. 3. Spindle Fiber Tension and the Reorientation of Mal-Oriented Chromosomes.” *The Journal of Cell Biology* 43, no. 1 (October 1969): 40–50.

Pearson, Chad G., Paul S. Maddox, E.D. Salmon, and Kerry Bloom. “Budding Yeast Chromosome Structure and Dynamics during Mitosis.” *The Journal of Cell Biology* 152, no. 6 (March 19, 2001): 1255–66. https://doi.org/10.1083/jcb.152.6.1255.

Santaguida, Stefano, and Andrea Musacchio. “The Life and Miracles of Kinetochores.” *The EMBO Journal* 28, no. 17 (September 2, 2009): 2511–31. https://doi.org/10.1038/emboj.2009.173.

Wisniewski, Jan, Bassam Hajj, Jiji Chen, Gaku Mizuguchi, Hua Xiao, Debbie Wei, Maxime Dahan, and Carl Wu. “Imaging the Fate of Histone Cse4 Reveals de Novo Replacement in S Phase and Subsequent Stable Residence at Centromeres.” *eLife* 3 (May 20, 2014). https://doi.org/10.7554/eLife.02203.

Yeh, Elaine, Julian Haase, Leocadia V. Paliulis, Ajit Joglekar, Lisa Bond, David Bouck, E.D. Salmon, and Kerry S. Bloom. “Pericentric Chromatin Is Organized into an Intramolecular Loop in Mitosis.” *Current Biology* 18, no. 2 (January 2008): 81–90. https://doi.org/10.1016/j.cub.2007.12.019.